Magma chamber behavior beneath a volcanic edifice

Virginie Pinel, Claude Jaupart

Magma chamber behavior beneath a volcanic edifice

Virginie Pinel and Claude Jaupart

Laboratoire de Dynamique des Systèmes Géologiques, Institut de Physique du Globe de Paris, Paris, France

Received 7 January 2002; revised 1 July 2002; accepted 6 July 2002; published 4 February 2003.

[1] The construction of a large volcanic edifice at Earth's surface generates stresses in the upper crust whose magnitude is comparable to those of tectonic stresses and overpressures within a magma chamber. We study how this affects eruption behavior. Analytical calculations are carried out in two dimensions for a cylindrical reservoir with an internal overpressure in an elastic half-space with an edifice at the surface. Different edifice shapes are considered, from shield volcanoes with gentle slopes to stratovolcanoes with steeper flanks. Without an edifice at the top, the hoop stress at the cavity walls reaches a maximum at two symmetrical points at some distance from the axis, away from the top of the chamber. With an edifice at the top, the maximum is reached at the top of the chamber, just beneath the edifice summit. This implies preferential failure of chamber walls at the axis and hence the focussing of volcanic activity through a central vent system. Tensile failure of the cavity walls occurs for a critical value of magma overpressure which depends on the dimensions of the edifice and on the depth and size of the cavity. For a small magma chamber beneath a large stratovolcano, the magmatic overpressure at the onset of eruption increases as the edifice grows and decreases following edifice destruction. These effects may explain why pressures recorded in phenocryst assemblages at Mount St. Helens, have varied over the past 4000 years as the edifice went through successive phases of growth and destruction. *INDEX TERMS:* 8164 Tectonophysics: Evolution of the Earth: Stresses—crust and lithosphere; 8414 Volcanology: Eruption mechanisms; 8434 Volcanology: Magma migration; *KEYWORDS:* volcanic edifice, magma transport, magma chamber pressure, vent location

Citation: Pinel, V., and C. Jaupart, Magma chamber behavior beneath a volcanic edifice, *J. Geophys. Res.*, *108*(B2), 2072, doi:10.1029/2002JB001751, 2003.

1. Introduction

[2] The structure and dimensions of volcanic plumbing systems, defined to be the system of connected reservoir(s) and conduit(s) which channels magma to Earth's surface, remains largely unknown despite repeated efforts. For example, there is still considerable debate about the structure and size of the magmatic plumbing system beneath Mount St. Helens [*Lees*, 1992; *Moran*, 1994; *Blundy and Cashman*, 2001]. According to *Rutherford and Devine* [1988], the May 1980 magma crystallized at a pressure of about 220 MPa, corresponding to lithostatic conditions at a depth of about 8 km. This may be compared to independent seismological estimates. On the one hand, seismic tomography suggests the existence of a shallow storage zone between 3.5 and 6.0 km and of a larger reservoir at 9 km below sea level [*Lees*, 1992]. On the other hand, local seismicity delineates a reservoir at a depth of about 6.5 km [*Barker and Malone*, 1991; *Moran*, 1994]. These different estimates can hardly be considered consistent with one another and generate considerable difficulties when studying eruptive behavior. In a "typical" model of a volcanic system, a magma reservoir feeds eruptions at regular intervals due to cristallisation or to replenishment from a deeper magma source [*Tait et al.*, 1989]. Thus the magma chamber volume affects the frequency and volume of eruptions. In addition, the size and depth of a reservoir are key factors for the rates of magma differentiation and volatile exsolution, as well as for the stress field due to magmatic overpressure. For example, for a spherical reservoir beneath a free surface, wall failure occurs at some distance from the axis of symmetry, away from the top of the reservoir [*Jeffery*, 1920; *McTigue*, 1987].

[3] This short discussion explains why it is essential to determine the location and size of magma reservoir(s) beneath an active volcano. An even more important goal is to assess whether the same reservoir feeds several eruptions in a row, which can only be achieved through petrological studies of past eruption products. At Mount St. Helens, petrological pressure estimates for the main eruptions of the last 4000 years vary significantly, from about 160 to 300 MPa [*Gardner et al.*, 1995] (Figure 1). Even more surprising is the fact that pressure may change very rapidly, sometimes in a few years only. *Gardner et al.* [1995] have argued that magmatic overpressures cannot reach large values and hence that petrological pressure estimates are close to lithostatic values. They have therefore ruled out the simple model of a fixed reservoir and have suggested that the Mount St. Helens reservoir has moved through the crust.

0148-0227/03/2002JB001751$09.00

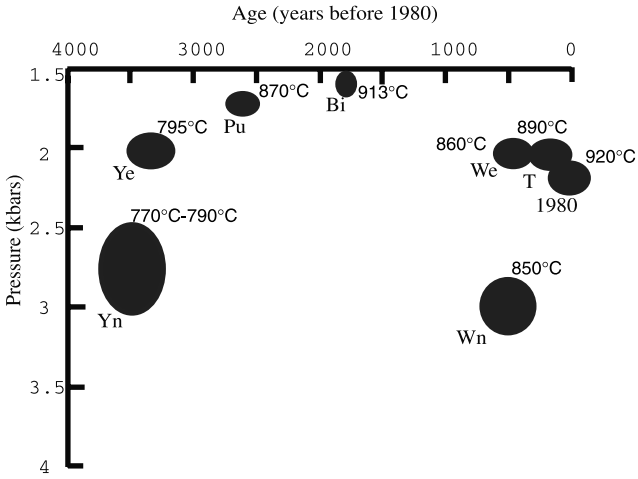

Figure 1. Pressure values deduced from phenocryst assemblages in erupted lava samples for several explosive eruptions at Mount St. Helens (data from *Gardner et al.*, [1995]). Symbol size is proportional to total erupted volume. Pressure determinations are within ±0.4 kbar. Note the very large and rapid pressure drop following the two largest explosive eruptions, Yn and Wn. The Wn and We eruptions are separated by only a few years.

[4] From a more general perspective, it is now clear that many different variables are required to account for the structure and long-term evolution of volcanic plumbing systems. *Hildreth* [1981] and *Bacon* [1985], for example, have drawn attention to the regional stress field and to the magma supply rate. Surprisingly, one component of volcanic systems has received scant attention: the edifice at Earth's surface. Yet this part of the system obviously induces large stresses in the upper crust. A stratovolcano frequently exceeds 2 km in height, corresponding to a surface load of more than 50 MPa. Thus it is responsible for stress changes in the upper crust that are comparable to, and may be greater than, tectonic stresses [*Van Wyk de Vries and Matela*, 1998]. The induced stress field affects dike propagation toward Earth's surface and may prevent the eruption of primitive magmas [*Pinel and Jaupart*, 2000]. One crucial feature is that it may change rapidly due to modifications of edifice size. For example, at both Santorini, Aegean Sea, and Anak Krakatau, Indonesia, edifices have grown to heights of several hundred meters in a few hundred years. A volcanic edifice may also get destroyed by magmatic intrusion, phreatic explosion, crater excavation or landslide [*Siebert et al.*, 1987; *Hausback and Swanson*, 1990].

[5] In the present paper, we investigate how the growth of an edifice affects a reservoir of magma in the upper crust. We use a two-dimensional elastic model to determine the location of fractures on the chamber walls and to calculate the values of magmatic overpressure required to start an eruption. The paper closes with a discussion of volcanological implications.

2. Elastic Model

2.1. General Description

[6] Models involving a magma reservoir have been used frequently to interpret deformation data during eruptive episodes. Most calculations rely on the Mogi model for a point source in an elastic half-space [*Mogi*, 1958], and there have been few attempts at more complicated reservoir dimensions and shapes [*Okada*, 1985; *Davis*, 1986; *McTigue*, 1987]. Here, we are interested in specifying eruption conditions, which requires knowledge of the internal magma pressure when the reservoir walls fail as well as the location of fractures along the walls. To achieve this aim, we study the behavior of a cavity of finite size which is subjected to changes of magmatic pressure and to the growth of an edifice at the surface.

[7] The theoretical model solves for elastic stress and deformation in two space dimensions (x, z) (Figure 2). The sign convention is such that tensile stresses are negative. The upper crust is characterized by Poisson's ratio ν and rigidity G. The volcanic edifice is a slab or a cone of radius R_e and height H_e. The magma chamber is cylindrical in shape with radius R_c at depth H_c. The reference state before loading is the lithostatic stress field, such that there is no edifice at the surface and that the magma reservoir lies in a neutral buoyancy zone, where magma and country rock have the same density ρ_m. All calculations in this paper deal with perturbations from this reference state (Figure 3). In the liquid-filled reservoir, no long-term deviatoric stresses can be sustained and the pressure gradient must be hydrostatic. For neutral buoyancy conditions, this pressure gradient is equal to the lithostatic gradient. Thus the pressure field within the reservoir is constrained to remain equal to the lithostatic pressure field plus some overpressure ΔP, which will be called the magmatic overpressure.

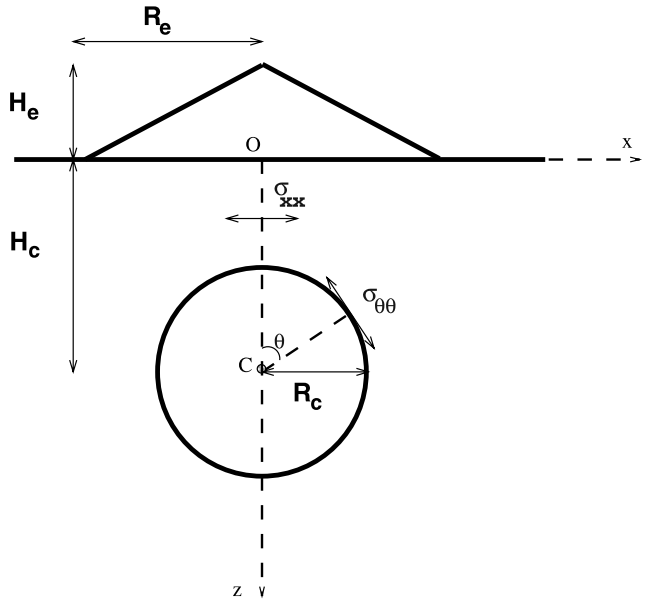

Figure 2. Geometrical setup for the problem. A cylindrical reservoir of radius R_c is located at depth H_c beneath a volcanic edifice. Angle θ is measured with respect to the vertical axis of symmetry. $\sigma_{\theta\theta}$ stands for the hoop stress on the reservoir walls. The volcanic edifice may be either a stratovolcano with steep slopes ($\gamma = H_e/R_e = 0.6$) or a shield volcano with gentle slopes ($\gamma = H_e/R_e = 0.1$).

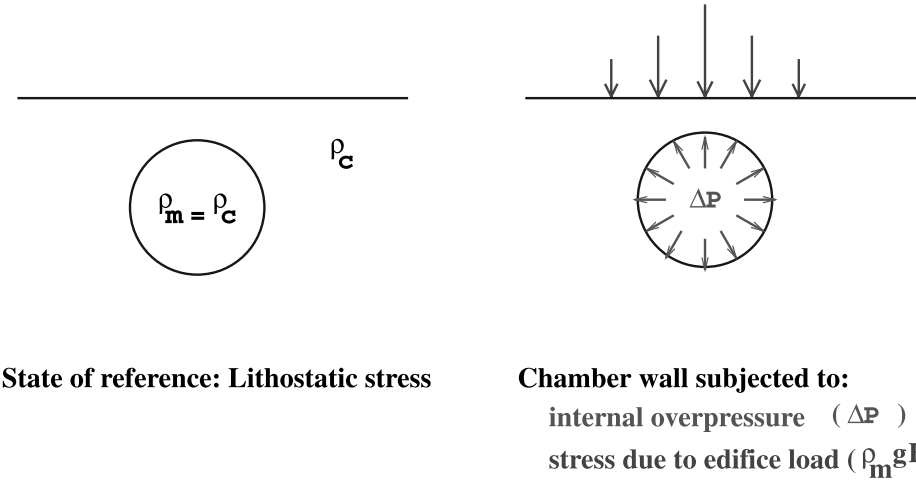

Figure 3. Stresses involved in the problem. (left) Reference stress field, such that a neutrally buoyant magma reservoir lies in a lithostatic stress field. (right) Stress perturbations whose effects on the surrounding elastic medium are solved for: a magmatic overpressure ΔP in the reservoir and a load due to an edifice at Earth's surface. The problem is split into two independent problems which are solved separately. The first problem is the classical one of an overpressured cavity beneath a stress-free surface. The second problem is a reservoir with zero internal overpressure and a surface load.

[8] The problem has three dimensionless parameters which define the different dimensions involved:

$$a_c = \frac{R_c}{H_c}, \tag{1}$$

$$a_e = \frac{R_e}{H_c}, \tag{2}$$

$$\gamma = \frac{H_e}{R_e}. \tag{3}$$

These stand for the reservoir radius, the edifice radius and the edifice thickness, respectively. For a conical edifice, γ is the slope of the flanks and will be set equal to values of 0.1 and 0.6, corresponding to a shield volcano with gentle slopes and to a stratovolcano with steep flanks, respectively.

[9] Calculations for a flat edifice (slab-shaped) are detailed in Appendix A. Solutions for a conical edifice are obtained by adding slabs of infinitesimal thicknesses. Two different problems are solved separately: one deals with the edifice load and zero reservoir overpressure, and the other deals with magma overpressure and zero surface load. In this section, we shall briefly describe the main features of both problems.

2.2. Model Validation

[10] Our calculations rely on the determination of the stress function χ for different boundary conditions (Appendix A). *Jeffery* [1920] showed that provided the applied forces taken as a whole are in equilibrium, which is always true here, the stress function χ is uniquely determined. This stress function is the solution of the biharmonic equation which, by construction, is the necessary and sufficient condition for mechanical equilibrium as well as for compatibility with the elastic constitutional equations. To verify that there were no errors in the analytical formulae for series expansions, numerical values for all stress components were used in a finite difference scheme to check for mechanical equilibrium, and convergence was systematically verified.

[11] We have further verified that our calculations are correct in several well-known limit cases. In the limit of a small reservoir beneath a large slab-shaped edifice ($a_c \to 0$ and $a_e \to \infty$), the reservoir must behave as if it was in an infinite medium subjected to a uniform far-field pressure equal to the edifice load, $\rho_m g\ H_e$. Solutions for zero wall deformation may be found in [*Love*, 1944]

$$\sigma_{rr} = 2(1-\nu)\rho_m g H_e, \tag{4}$$

$$\sigma_{\theta\theta} = 2\nu\rho_m g H_e. \tag{5}$$

We find that, as the edifice radius increases (as $a_e \to \infty$), both stress components tend to these limits (Figure 4). The same is true for the hoop stress at the reservoir walls, $\sigma_{\theta\theta}$. In the same limit of small reservoir and large edifice (small a_c and large a_e), the normal stress σ_{xx} at the axis (i.e., for $x = 0$) is expected to remain equal to the surface value, $\rho_m g\ H_e$, over a large depth interval above the reservoir (Figure 5).

[12] Another verification may be obtained by considering the case of a large reservoir at shallow depth beneath a small edifice ($a_c \approx 1$). If the edifice radius is much larger than the thickness of rocks above the reservoir ($1 - a_c \ll a_e \ll a_c$), the roof region behaves as a thin elastic plate. Thus we expect that, at the axis, the horizontal normal stress, σ_{xx}, varies linearly with depth and changes sign in the middle of the plate. Our solution indeed behaves in this manner (Figure 6).

2.3. Stresses Due to Magma Overpressure

[13] The solution for zero surface load and magmatic overpressure ΔP is well known [*Jeffery*, 1920] (Figure 7). In this case, the hoop stress at the reservoir wall is given by

$$\sigma_{\theta\theta}(\theta) = -\frac{\Delta P}{1-a_c^2}\left[1 + a_c^2 - 2a_c^2\left(\frac{a_c - \cos\theta}{1 - a_c\cos\theta}\right)^2\right], \tag{6}$$

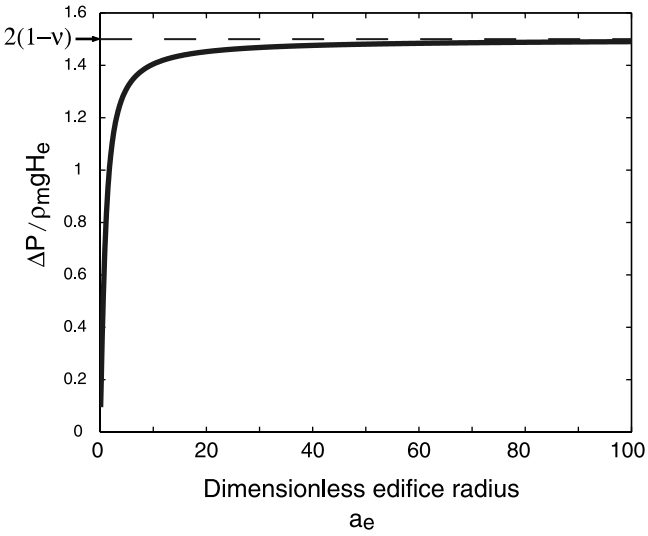

Figure 4. Magmatic overpressure required to achieve zero displacement of the reservoir walls beneath an edifice, as a function of dimensionless edifice radius a_e (equal to R_e/H_c). Calculations are made for a slab. The dimensionless reservoir radius ($a_c = R_c/H_c$) is set at 0.01. The overpressure tends to the constant value $2(1 - \nu)\rho_m g H_e$ corresponding to the analytical solution for a cavity in an infinite medium.

where θ is the polar angle (Figure 2). In this case, the hoop stress at the wall is tensile everywhere. Tension is minimum at the points nearest to and farthest from the surface ($\theta = 0, \pi$, respectively), where it is equal to the magma overpressure. Wall tension is maximum at a value σ_m at two symmetrical points away from the axis, for $\theta = \theta_m$ such that

$$\cos\theta_m = a_c. \tag{7}$$

This angle corresponds to locations on the chamber walls such that the tangents pass through point O in Figure 2. The maximum tensile hoop stress is equal to:

$$\sigma_m = -\Delta P \frac{1 + a_c^2}{1 - a_c^2} \tag{8}$$

which tends to infinity when $a_c \rightarrow 1$, i.e., when the reservoir is brought closer and closer to the surface. σ_m increases as the reservoir depth decreases because of stress concentration in a roof region of decreasing thickness. Finally, one may note that σ_m tends to $-\Delta P$ as $a_c \rightarrow 0$, i.e., as the reservoir size decreases. In this limit, the reservoir behaves as if it was in an infinite medium.

2.4. Hoop Stresses on the Chamber Walls Due to Edifice Load

[14] The complementary problem to the one above is that of a liquid-filled reservoir beneath an edifice. With respect to the reference state, we impose zero reservoir overpressure and a load at the surface. Using the principle of superposition, this solution can then be added to the previous one to tackle arbitrary values of surface load and magmatic overpressure. For simplicity, in this section, calculations are discussed, and results shown, for a slab-shaped edifice only.

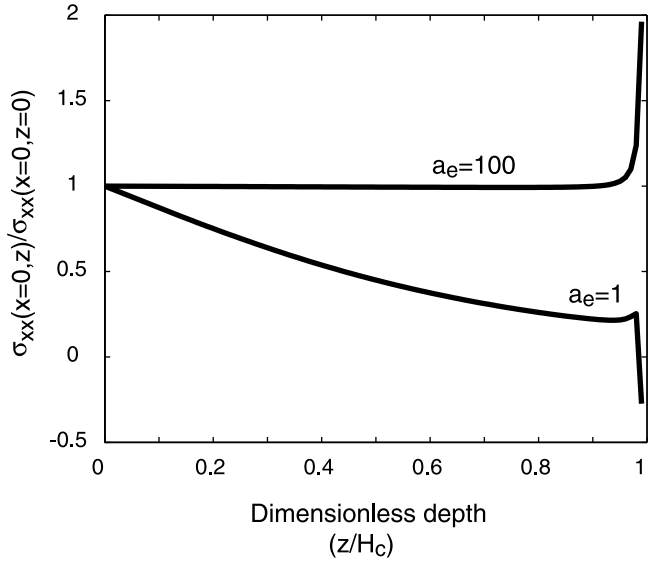

Figure 5. Horizontal normal stress σ_{xx} on the axis as a function of depth due solely to the edifice load at Earth's surface for a small reservoir ($a_c = R_c/H_c = 0.01$). Calculations are made for a slab. Two curves are shown for two values of the dimensionless edifice radius $a_e = R_e/H_c$. For large a_e, the edifice generates compression over a large depth range and normal stress σ_{xx} remains constant at shallow depth above the reservoir.

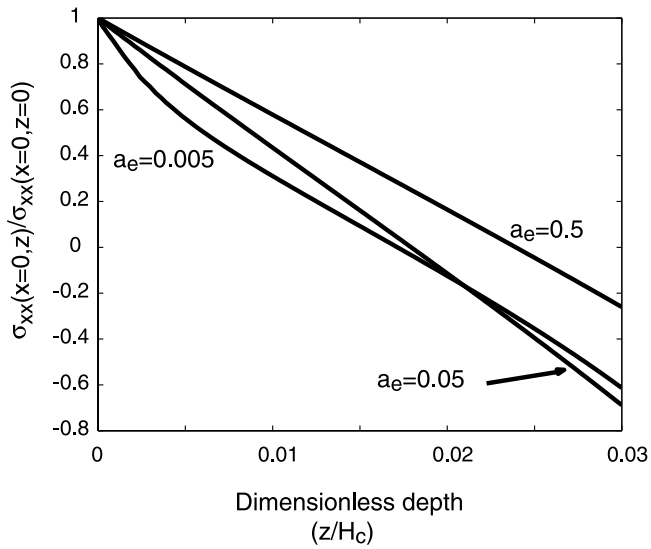

Figure 6. Horizontal normal stress σ_{xx} on the axis as a function of depth due solely to the edifice load at Earth's surface for a large reservoir ($a_c = R_c/H_c = 0.97$). Calculations are made for a slab. Three curves are shown corresponding to three different edifice sizes. For small values of a_e, the reservoir roof is thin and behaves as an elastic plate. For very small values of a_e (0.005), the edifice load is taken up by deformation in the upper part of the roof implying a small tensile stress on the reservoir wall. For intermediate values of a_e (0.05), the roof region behaves as a thin elastic plate and normal stress σ_{xx} decreases linearly with depth.

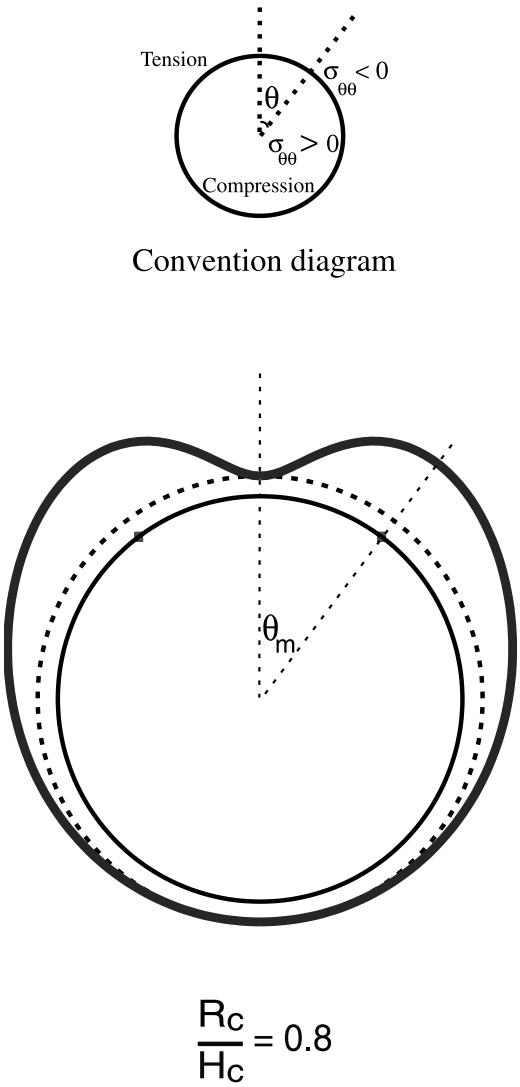

Figure 7. Angular distribution of hoop stress (thick plain curve) around the reservoir walls for the first elastic problem (magmatic overpressure and no edifice at the surface). Stress values are scaled by the magmatic overpressure ΔP and are shown as a function of angle θ for $a_c = R_c/H_c = 0.8$ (Figure 2). The top part of the diagram shows the convention used to draw the figure: compression and tension appear as negative and positive stresses, respectively (contrary to the sign convention used in the calculations). The thin plain circle corresponds to zero stress, and the dashed line shows a uniform tension of 1 corresponding to the solution in an infinite medium. The hoop stress is maximum for $\theta = \theta_m$ such that $cos\theta_m = a_c$.

In this case, the edifice height H_e enters the problem through a scale factor for stresses, and only two independent parameters are involved, a_c and a_e.

[15] Hoop stress values on the reservoir walls are shown in Figure 8 for different values of a_c and a_e. The solutions can be understood using the solution in a half-space without a reservoir. In this case, stresses due to the edifice are compressive near the top and decrease with increasing depth, becoming negligible at depths larger than about 3 R_e. With a reservoir present, there are two simple end-member behaviors for extreme values of a_e and a_c, the dimensionless edifice and reservoir radii. For small values of a_e and large values of a_c, the edifice acts as a narrow load on the reservoir roof and induces bending, which generates tensile stresses at the top of the reservoir. For large values of a_e and small values of a_c, the edifice generates compression over a large volume encompassing the whole reservoir, inducing compression everywhere on the walls.

[16] For a more detailed look at these solutions, we focus on the hoop stress at the top of the reservoir (i.e., for $\theta = 0$) (Figure 9). For small values of a_e, the edifice induces stresses over a region of small vertical extent. In this case, the load gets compensated by deformation within the roof region only and the stress at the top of the reservoir is a small fraction of the surface load. The hoop stress at the top is tensile with a dimensionless magnitude smaller than 1. As the edifice radius is made larger, deformation affects an

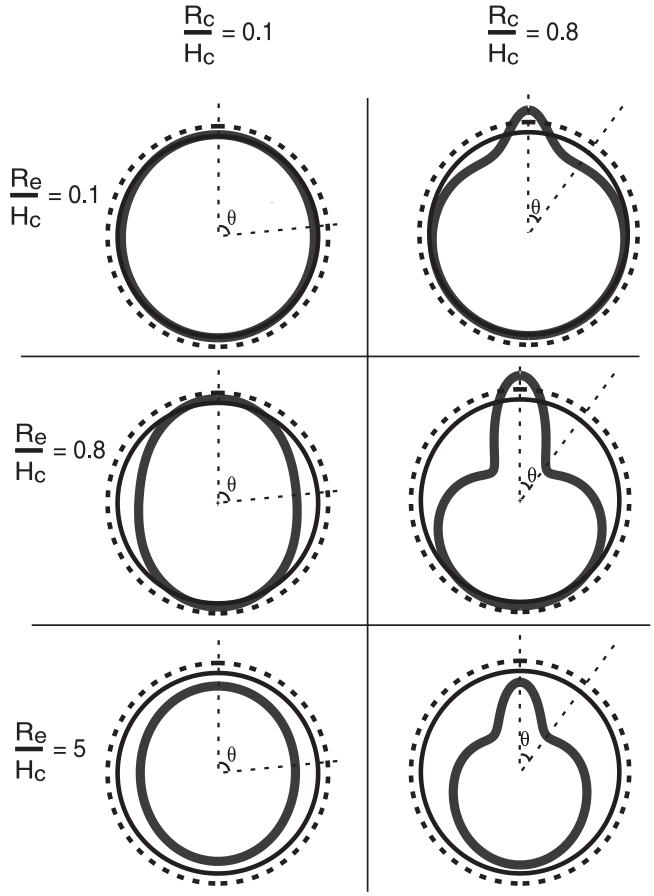

Figure 8. Angular distribution of hoop stresses at the walls of the reservoir due to the load of volcanic edifice at Earth's surface with zero magmatic overpressure. Stress values are scaled to the weight of the edifice, $\rho_m g H_e$. The diagram uses the same convention than Figure 7. Two sets of results are shown for various values of reservoir radius a_c and edifice radius a_e. Note the large difference between the results for small a_c (left-hand side) and a_c close to 1 (right-hand side). For small a_c, the edifice induces compression. For a_c close to 1 and for a_e smaller than about 1, the edifice induces bending in the thin roof above the reservoir, which generates local tension at the axis.

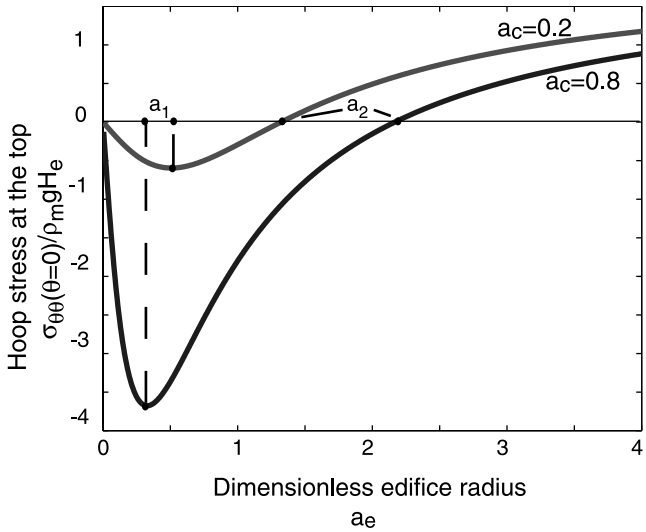

Figure 9. Largest hoop stress at the top of reservoir as a function of edifice radius a_e. Stress values are scaled to the edifice load $\rho_m g\, H_e$. Curves are shown for different values of reservoir size a_c. For small values of a_e, the hoop stress is tensile and increases with edifice size. For given a_c, the dimensionless tensile hoop stress reaches a maximum for some critical value of edifice radius, denoted a_1. This maximum dimensionless hoop stress value increases with increasing a_c. The hoop stress changes sign for a_e equal to a second critical value denoted a_2 and becomes compressive for larger values of a_e. The dimensionless hoop stress tends to 2 as $a_e \rightarrow \infty$.

increasingly thicker part of the roof region and the hoop stress is tensile with an increasing magnitude. For a reservoir located close to the surface (a_c close to 1), the hoop stress at the top may become much larger than the load itself because stresses get concentrated in the thinnest part of the roof. Above a certain critical value of the edifice radius, deformation is no longer limited to the thin part of the roof at the top and involves a larger lateral extent. Thus there is less bending deformation. In this second regime, the hoop stress is still tensile but decreases as a function of edifice radius. For given reservoir, there is therefore a critical value of the edifice radius, noted a_1, for which the dimensionless tensile hoop stress has a maximum. As the edifice radius is increased further, the surface load induces compression over an increasingly large region. There is therefore a third regime for which the hoop stress at the top is no longer tensile. The change of behavior from tension to compression is achieved for a second critical value of a_e, noted a_2, which is of order 1 (Figure 9). As a_e tends to infinity, the reservoir behaves as if it was subjected to a uniform far-field confining pressure in an infinite medium. The hoop stress at the top tends to the dimensionless value of 2, as predicted by theory [*Love*, 1944]. These results emphasize that wall stresses can be significantly larger than the edifice load in both tension and compression.

[17] We have defined two critical values of the edifice radius which separate three different deformation regimes for the roof region. What matters is the depth over which the surface load can be compensated, and hence the two critical values take values of order 1. The two critical values have different behaviors as a_c increases: a_1 decreases whereas a_2 increases (Figures 9 and 10). The magnitude of tensile stresses depends on the reservoir size a_c (Figures 8 and 9). For values of a_c close to 1, the roof region is thin and tensile stresses may be very large. For small values of a_c, the thick roof can sustain large loads, implying small tensile stresses.

[18] Magma overpressure always generates tension, whereas the edifice may be responsible for tension or compression depending on the values of a_e and a_c. Thus the effects of magma overpressure and edifice load may counteract one another and lead to complex stress distributions at the reservoir walls. For practical purposes, the most significant result is that, beneath a large edifice, large values of magmatic overpressure are required to put the reservoir walls in tension.

2.5. Displacements of the Chamber Walls

[19] As regards displacements, the situation is simpler. Magma overpressure always acts to increase the reservoir volume. The amount of expansion is

$$\frac{\Delta V}{V} = \frac{\Delta A}{A} = \frac{\Delta P}{G\sqrt{1-a_c^2}}\left[2(1-\nu) - (1-2\nu)\sqrt{1-a_c^2}\right]. \quad (9)$$

The edifice load always has the opposite effect, that is, it diminishes the reservoir volume.

[20] Let us first consider the effect of magma overpressure alone. For small a_c, the reservoir is small compared to its depth, and the situation is close to that for a cavity in an infinite medium. In this case, the reservoir inflates in an isotropic way and the radial displacement tends to a uniform value of $[a_c \Delta P]/2G$. As a_c increases, the reservoir roof gets thinner and deformation becomes more complicated. For a_c close to 1, the reservoir tends to become elongated in the vertical direction.

[21] The effect of the edifice load is illustrated in Figure 11, again for slab-shaped edifices. For all cases shown,

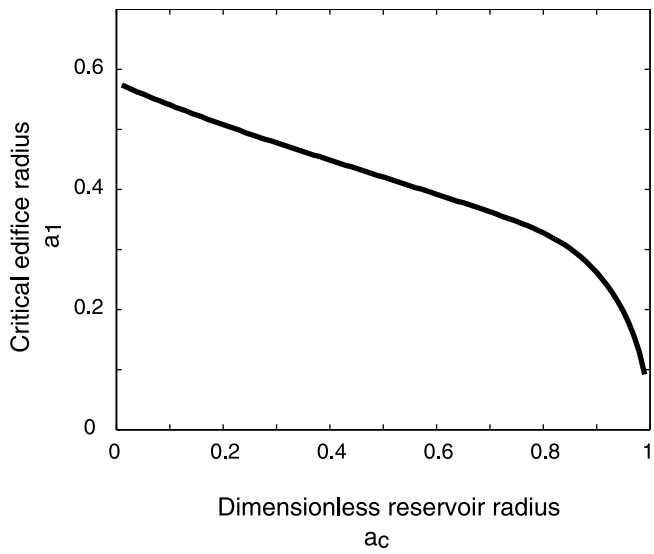

Figure 10. Critical value a_1 of the dimensionless edifice radius a_e for which the magnitude of the tensile hoop stress reaches a maximum (see Figure 9), as a function of dimensionless reservoir size a_c.

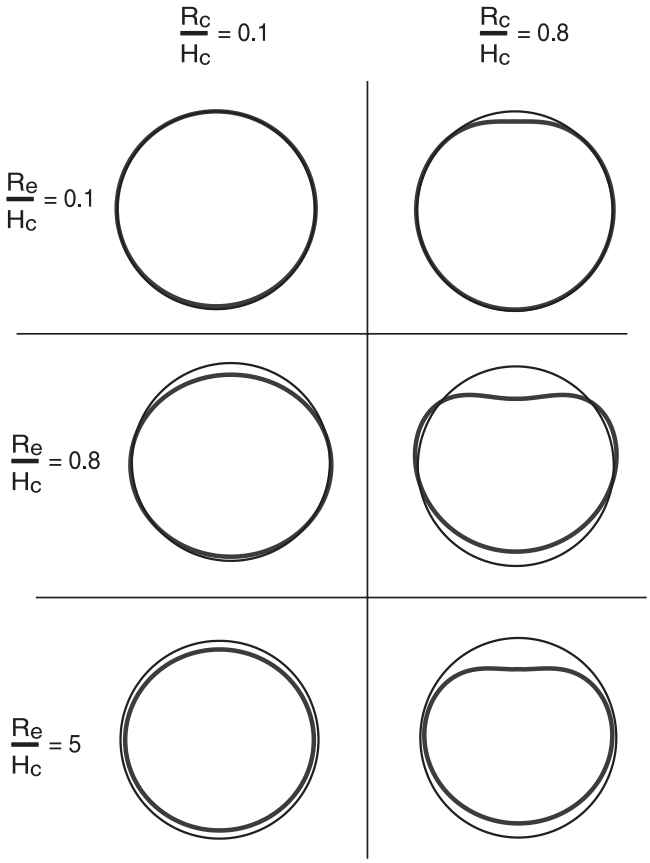

Figure 11. Displacement of the reservoir walls for the same cases illustrated in Figure 8. Displacement values have been multiplied by a factor of 5. Note the different results for small and large reservoir radii.

values for the edifice load, $\rho_m g H_e$, and rigidity G have been set equal to values of 2×10^7 and 10^9 Pa, respectively. For small reservoirs (small values of a_c), the edifice acts to flatten the reservoir. For large reservoirs (large values of a_c), the thin roof region deforms markedly.

3. Eruption Conditions

[22] In the following, we consider conical edifices and consider two different values of volcano slope, corresponding to shield volcanoes ($\gamma = 0.1$) and stratovolcanoes ($\gamma = 0.6$). For given edifice radius R_e, the smaller γ, the smaller the depth range over which stresses are compressive.

3.1. Failure Criterion

[23] We only consider tensile failure such that magma intrudes a crack forming at the reservoir walls. We adopt a simple rupture criterion, such that the magnitude of the deviatoric stress exceeds some threshold value T_s, which may be called the tensile strength of the rocks. This is equivalent to the well-known Terzaghi condition [e.g., *Valko and Economides*, 1995, p. 65].

[24] Along the reservoir walls, the normal stress is, by continuity,

$$\sigma_{rr} = \Delta P. \tag{10}$$

In an infinite medium, the hoop stress due to magma overpressure is constant along the wall:

$$\sigma_{\theta\theta} = -\Delta P\,. \tag{11}$$

Thus the stress perturbation is purely deviatoric, with no pressure component. In a half-space, this is only longer true for $\theta = 0$ or $\theta = \pi$ (see equation (6)), and the stress perturbation tensor is no longer purely deviatoric.

[25] In the present model, the perturbation stress tensor takes the following form:

$$\begin{pmatrix} \sigma_{rr} & 0 \\ 0 & \sigma_{\theta\theta} \end{pmatrix}, \tag{12}$$

such that $\sigma_{rr} + \sigma_{\theta\theta} \neq 0$. The reference stress field has no deviatoric component, and hence the deviatoric stress tensor is

$$\begin{pmatrix} \frac{\Delta P - \sigma_{\theta\theta}}{2} & 0 \\ 0 & \frac{\sigma_{\theta\theta} - \Delta P}{2} \end{pmatrix}. \tag{13}$$

In this case, the tensile failure criterion becomes

$$\frac{\sigma_{\theta\theta} - \Delta P_c}{2} = -T_s\,, \tag{14}$$

where ΔP_c is the critical overpressure for failure. As the reservoir size decreases, this criterion tends to the following simple form:

$$\Delta P_c \rightarrow T_s \text{ when } a_e \rightarrow 0 \text{ and } a_c \rightarrow 0. \tag{15}$$

[26] In practice, dike initiation from a pressurized reservoir must be viewed as a dynamical process such that magma pressure is large enough to drive flow into the incipient fracture so that a crack begins to propagate. For viscous magmas such as dacites and rhyolites, viscous stresses are important and it is more useful to define an "effective" tensile strength which is larger than the intrinsic material property T_s [*McLeod and Tait*, 1999].

[27] In the following, we are only interested in cracks opening in the upper part of the reservoir; that is, we ignore those which may develop near the base. All the physical properties involved are listed in Table 1 together with the numerical values adopted for illustration purposes.

Table 1. Parameters and Physical Properties Used in the Calculation

Parameters/Properties	Symbol	Value
Geometrical parameters		
Depth of the reservoir	H_c	
Radius of the reservoir	R_c	
Radius of the volcano	R_e	
Height of the volcano	H_e	
Physical properties		
Poisson's ratio	ν	0.25
Rigidity, Pa	G	1×10^9
Tensile strength, Pa	T_s	2×10^7
Density of the magma, kg m^{-3}	ρ_m	2700
Dimensionless numbers		
	$a_c = R_c/H_c$	
	$a_e = R_e/H_c$	
	$\gamma = H_e/R_e$	

3.2. Fracture Location

[28] Wall rupture is achieved for some value θ_r of angle θ, implying that dikes are generated at specific locations in the reservoir. Without any edifice, $\theta_r = \theta_m$ (equation (7)) and the critical magma overpressure for eruption is

$$\Delta P_c = T_s \left(1 - a_c^2\right), \tag{16}$$

which is smaller than T_s. With increasing a_c, rupture occurs at increasingly smaller values of overpressure because of stress concentration in a roof of decreasing thickness.

[29] As explained above, an edifice may generate tension or compression on the reservoir walls depending on its size. In the former case, tensile stresses at the wall are largest for $\theta = 0$, i.e., at the top of the reservoir, beneath the edifice summit. Adding the effects of magma overpressure leads to a complicated stress field, and it is useful to think in terms of a given reservoir under edifices of increasing dimensions. Beneath a small edifice, the stress field is dominated by the effect of magma overpressure and dikes may be generated away from the edifice. A large edifice always acts to localize rupture at the top of the reservoir. For values of a_e below the critical value a_2, this result is obvious because the surface load generates tension on the reservoir walls with a maximum value at the top. For values of a_e above this critical value, the surface load induces compression on the reservoir walls and tensile stresses are due to magmatic overpressure only. The largest net tension shifts to the top of the reservoir because the load-induced compression is smallest there (Figure 8).

[30] Rupture locations depend on edifice size and shape and reservoir size. The edifice shape comes into play because its affects the scale of deformation: induced stresses decrease over increasingly smaller distances in both the vertical and horizontal directions as γ increases. Three cases may be defined according to the value of θ_r: (1) $\theta_r \leq \theta_m$, i.e., closer to the axis than in the absence of an edifice, (2) $\theta_r = 0$, i.e., at the top of the reservoir, and (3) $\theta_r > \theta_m$, i.e., farther from the axis than in the absence of an edifice.

[31] Mature volcanic edifices have typical dimensions of several kilometers, implying that a reservoir with radius <1 km may be considered small in our context. For the purposes of illustration, we first consider a "small" reservoir with R_c = 200 m (Figures 12a and 12b). Beneath small edifices, the rupture angle θ_r remains close to the reference value θ_m. Beneath a shield volcano (γ = 0.1), the rupture angle varies over a large range as a function of reservoir depth and depends weakly on edifice size (Figure 12a). In a shallow reservoir (a_c larger than about 0.4), the rupture angle is never zero, implying that eruptive vents remain at the same distance from the central region throughout the history of the volcano. In a deep reservoir (a_c smaller than about 0.4), the edifice generates compression, and wall rupture is achieved at the top, i.e., for $\theta_r = 0$. Reservoir behavior is markedly different beneath a stratovolcano (γ = 0.6, Figure 12b). With steeper flanks, the edifice may generate bending stresses on the roof even if the reservoir is small. Thus, as soon as there is an edifice of significant size (more than a few hundred meters in radius), the rupture angle is zero.

[32] Next, we consider a "large" reservoir such that R_c = 4 km (Figures 13a and 13b). Stresses due to the edifice vary significantly on the scale of the reservoir and one may not think simply in terms of superimposing two effects at the top of the reservoir. For small edifices, the magma overpressure effect dominates but the top part of the reservoir strongly deforms. The rupture angle is larger than θ_m, implying that dikes are issued from the sides of the reservoir. Above some threshold value of the edifice radius, the effect of the surface load eventually dominates and the rupture angle jumps to zero. In this case, there is no solution with values of the rupture angle θ_r between θ_m and 0. All else being equal, the threshold edifice size is smaller for a stratovolcano than for a shield volcano.

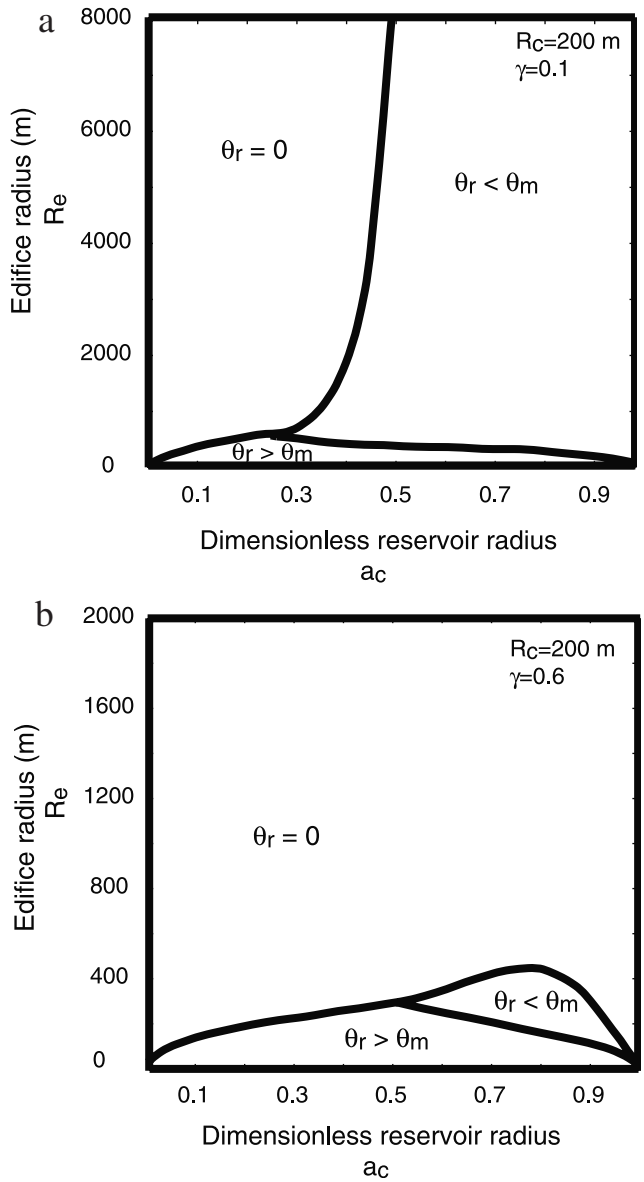

Figure 12. Values of the rupture angle θ_r where the reservoir wall fails in tension for a small reservoir (R_c = 200 m), as a function of edifice radius and dimensionless reservoir size a_c. (a) Shield volcano with gentle slopes (γ = 0.1). (b) Stratovolcano with steep slopes (γ = 0.6).

3.3. Overpressure in the Chamber

[33] In the following, we focus on stratovolcanoes (γ = 0.6). The critical magma overpressure ΔP_c at the onset of

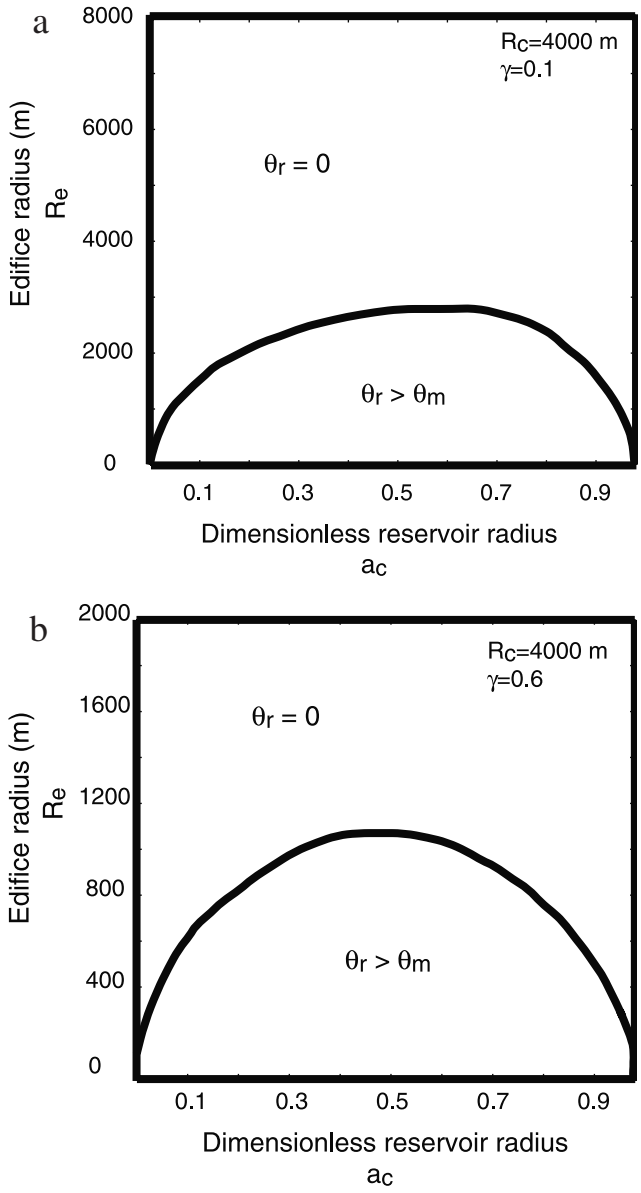

Figure 13. Same as Figure 12 with a large reservoir (R_c = 4000 m).

eruption depends strongly on edifice size. The change in overpressure increases as $a_c \rightarrow 1$ and we illustrate results for two values of a_c (Figures 14a and 14b). For small edifice radii, as explained above, the edifice load and magmatic overpressure have the same effect on the upper half of the reservoir walls. Furthermore, as the edifice grows, the magnitude of induced tensile stresses increases. Thus it takes smaller and smaller magmatic overpressures to generate an eruption. Above a critical value of R_e (corresponding to $a_e = a_1$, see Figure 9), the edifice starts to exert compressive stresses on the reservoir walls, and it takes larger and larger magmatic overpressures to generate an eruption. These two types of behavior are associated with different rupture locations along the reservoir walls. Fractures open away from the axis beneath a small edifice and at the axis beneath a large edifice. One should note that the critical value of magmatic overpressure for eruption may be much larger than the tensile strength of encasing rocks.

4. Volcanological Implications

4.1. Discussion

[34] In our model, the upper crust is assumed to behave elastically with no viscous stress relaxation. This is appropriate for the cold upper crust and for the short lifetimes of volcanic systems. Relaxation timescales have been estimated for the lithosphere as a whole, and are consistently larger than 5 Myr [*Beaumont*, 1981; *Nunn and Sleep*, 1984]. Such estimates must be considered as vertical averages and hence provide lower bounds for the upper crust where magma reservoirs are located. In comparison, Mount St. Helens is less than 50,000 years old [*Mullineaux*, 1986] and the more complicated Mount Adams system was active for about 500,000 years [*Hildreth and Lanphere*, 1994]. These observations suggest that an elastic model provides a reasonable approximation. Indeed, stratovolca-

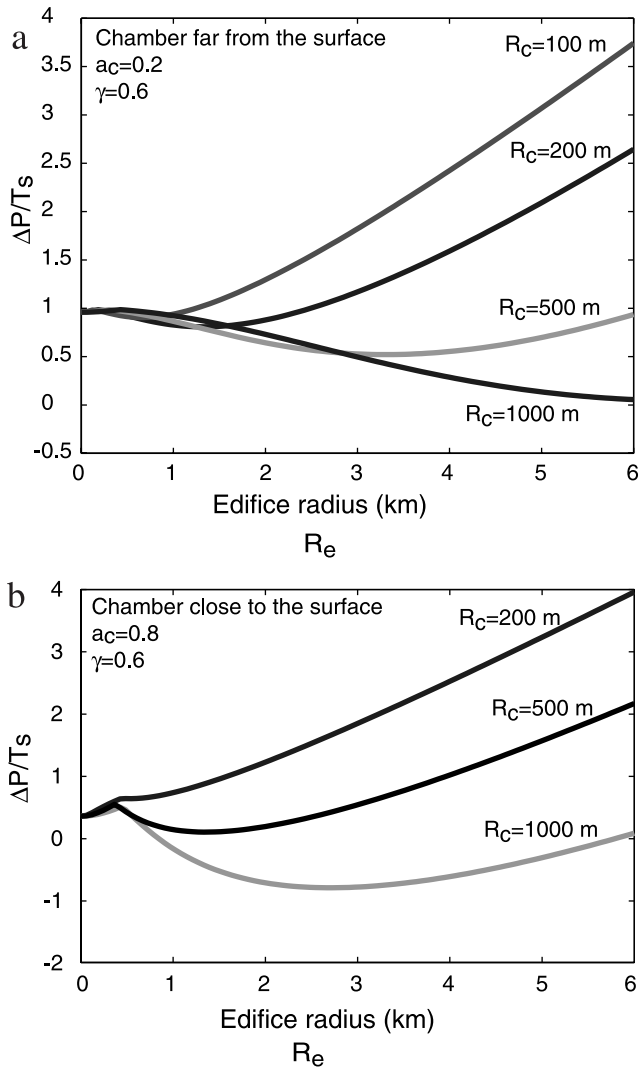

Figure 14. Critical magmatic overpressure for eruption as a function of edifice radius for a stratovolcano (γ = 0.6). (a) Results for a deep reservoir (a_c = 0.2). (b) Results for a shallow reservoir (a_c = 0.8).

noes are usually associated with positive free-air gravity anomalies, showing that their surface loads are not compensated [*Williams and Finn*, 1985]. On a smaller scale, rocks which are around the magma reservoir get heated up. Such local viscous behavior is limited to the thermal halo around the reservoir, which grows by heat diffusion. One should therefore introduce some "effective" reservoir size, which is slightly larger than that of the purely magmatic part.

[35] The model relies on a specific reservoir shape. A different shape would affect the quantitative results but not the main physical principles. For example, in a elastic half-space, the maximum hoop stress on the walls is reached at approximately the same location on the walls of a 2-D cylinder and a sphere, i.e., at angle θ_m given by equation (7) [*McTigue*, 1987; *Tsuchida et al.*, 1982]. The behavior of reservoirs with more complicated shapes may be understood using three principles. One is that a concentrated load acting on a thin roof induces bending, and hence tensile stresses at the top of the reservoir. A second principle is that the hoop stress due to magmatic overpressure depends on the local wall curvature. For a reservoir in the shape of a prolate spheroid, the maximum tensile stress due to magmatic overpressure is achieved at the top when the height/width ratio is larger than about 2 [*Tsuchida et al.*, 1982]. In this case, the effects of edifice load and magmatic overpressure reinforce one another to induce failure at the top for all edifice sizes. A third principle is that a large edifice generates compressive stresses over a large depth range. The bulk effect on the reservoir is an increase of internal pressure whose magnitude depends on the vertical extent of the reservoir. In Appendix B, we discuss the case of a reservoir with the shape of vertical crack and show that the liquid-filled volume acts as an integrating body which averages the externally imposed stress field.

[36] Detailed comparisons between model predictions and observations on a specific volcanic example are premature given the rather large errors on pressure estimates and reservoir location, as discussed below. It is clear that the model does not account for many complications which may arise in nature. The upper crust may be anisotropic and faulted. Results may be sensitive to reservoir shape, a point which we plan to investigate in a future paper. However, we have already explained that reservoirs with different shapes would have the same behavior than the cylindrical cavity studied here, and expect only quantitative differences. Another complication is that wall failure may not always ensure eruption at Earth's surface because, at shallow levels, the compressive stress field due to the edifice may halt dike ascent [*Pinel and Jaupart*, 2000]. A key variable is the magma volatile content and one may in fact calculate the minimum value required for a successful eruption. Such considerations are outside the scope of this paper.

[37] Below, we discuss eruptive behavior. The effects of the surface load are important only if the magmatic reservoir is not too deep. All mature stratovolcanoes have radii exceeding 4 km (about 5 km and 10 km for Mount St. Helens and Mount Adams, respectively, for example), implying that they affect the stress distribution in the upper crust over a depth range of more than 10 km. Most known magma reservoirs are located in this zone of influence. Two important points must be borne in mind. One is that stresses exerted on the walls of a reservoir may be significantly larger than the edifice load. The growth of a several kilometers high stratovolcano can cause pressure variations of as much as 100 MPa in a reservoir. The induced stresses may be larger than tectonic ones. The other point is that, depending on the location of there-servoir, the edifice may generate compressive or tensile stresses on the walls.

4.2. Distribution of Eruptive Vents

[38] The difficulty to locate magma chambers with geophysical techniques has led many authors to use other lines of reasoning. One such line of reasoning makes use of the distribution of eruptive vents at Earth's surface. Another line of reasoning relies on the composition and volume of erupted lavas and links the observed differentiation trend to the chamber size. Such chemical models require assumptions on the efficiency of mixing in reservoirs that simultaneously undergo differentiation, replenishment and eruption. These processes remain poorly understood, especially for reservoirs that contain viscous melts and that often become compositionally stratified. It is therefore useful to assess the physical evidence independently.

[39] We assume for the sake of argument that there is a magma reservoir at some depth which may or may not coexist with peripheral conduit systems connected to a deeper source of magma. This reservoir may also grow with time and one should account for this possibility. The model links the location of fractures opening at the reservoir walls to the sizes of the reservoir and of the edifice. In our calculations, fractures are generated at the reservoir walls at distance δ from the axis, such that

$$\delta = R_c \sin\theta_r. \tag{17}$$

Thus, as the rupture angle decreases to zero, wall fractures shift toward the axis. For small reservoirs, this shift may be gradual (Figures 12a and 12b). For large reservoirs, this shift occurs abruptly when the edifice reaches a certain size as the rupture angle jumps from values larger than θ_m to zero (Figures 13a and 13b).

[40] Beneath a small stratocone, $\theta_r > \theta_m$. In this case, dikes are issued from the sides of the reservoir where the local stress field is dominated by the effects of reservoir overpressure. Thus they initially follow a radial trajectory away from the axis. There is no mechanism to bring them back to the axis and the end result is a number of vents away from the focal region, at distances which may in fact be larger than δ. Beneath a mature stratovolcano, dikes are always generated at the top of the reservoir and cannot stray away from the axis in the stress field due to the edifice load [*Dahm*, 2000; *Muller et al.*, 2001]. In this case, eruptive activity gets automatically focused in the central region. Thus the distribution of eruptive vents together with a known edifice (or the lack of an edifice) leads to constraints on the size and depth of the reservoir.

[41] Large stratocones often arise from the central region of diffuse volcanic zones. In early stages of volcanic activity, primitive magmas erupt from fractures at the edges

of the reservoir (such that $\theta_r > \theta_m$). At Earth's surface, the associated vents would outline the reservoir in horizontal cross section. For such primitive lavas which are fluid and relatively volatile-poor, successive eruptions lead to a set of overlapping flows and domes which collectively build a lava shield. Regardless of the exact shape of such a shield, the diffusion-like character of elastic equations implies that the induced stress field at depth retains the same axial symmetry than the examples studied above, and the effects on the reservoir are the same. Above a certain height, or radius (Figure 13a), the lava shield or incipient edifice is sufficient to change the location of vents and to focus eruptive activity in the central region. Additionally, dikes rising through the stress field of such an edifice get deflected toward the axial region [*Dahm*, 2000]. In the present framework, therefore, edifice growth is a self-reinforcing process.

[42] A well-known feature of andesitic volcanic systems is that differentiated lavas seem to be confined to the focal region, i.e., erupt through a central vent system in the main stratocone, while primitive lavas may get erupted simultaneously through peripheral vents and fissures [e.g., *Hildreth and Lanphere*, 1994]. This has been attributed to the fact that primitive magmas rising in the central region are ''captured'' by a reservoir. This model is incomplete because it says nothing about the size of the reservoir and does not specify the connection between the deep supply system and the central vent complex. At Mount Adams, for example, the large stratocone lies at the center of a diffuse volcanic field extending over a radius of about 20 km [*Hildreth and Lanphere*, 1994]. The largest magma volumes were erupted in the focal region from central or proximal flank vents in the vicinity of the summit. The buildup of the edifice clearly went hand in hand with the focussing of eruptive activity, by definition, but was not necessarily due to the focussing of magma conduits from deep sources. As shown above, a magma reservoir would automatically sustain the central vent region.

[43] Some volcanic areas are characterized by a diffuse pattern of vents issuing evolved lavas. It has been argued that these provide evidence for large shallow reservoirs, on the assumption that vents can be generated over the whole surface of a reservoir [*Bacon*, 1985]. For example, the Glass Mountain-Long Valley system, which generated the enormous eruption of the Bishop Tuff, is laced with a large number of silicic vents over a broad region larger than the caldera itself [*Metz and Mahood*, 1985]. The system was active for more than 1 million years before the catastrophic Bishop Tuff event [*Metz and Mahood*, 1985]. The present-day caldera obviously demonstrates that a shallow magma chamber developed, but a key issue is to evaluate when it did develop. According to our model, if there had been a large reservoir in early stages, eruption of evolved magmas would have eventually been focused in the central region and a diffuse vent pattern could not have been sustained. This argument suggests that there was no large magma chamber in early stages of magmatic activity and hence that the reservoir grew with time. This is consistent with the chemistry of erupted lavas, which reflects mixing between primitive melt and evolved resident magma. Indeed, *Metz and Mahood* [1991] have suggested that the reservoir was smaller in early stages. There is a gradual evolution toward slightly more primitive compositions. As regards the reservoir, this requires that the input from the primitive source exceeds output toward the surface, which implies reservoir growth.

4.3. Mount St. Helens Magma Reservoir

[44] At Mount St. Helens, petrological studies indicate large pressure changes of more than 100 MPa, from 160 to 300 MPa over 4000 years [*Gardner et al.*, 1995] (Figure 1). Such pressure changes are significantly larger than experimental errors of about 40 MPa. This error level makes it difficult to tie down precisely the magnitude of pressure variations, but it is clear that pressure changed because the phase assemblages did evolve. At Mount St. Helens, a systematic trend is that the more evolved the magma, the larger the pressure [*Hopson and Melson*, 1990; *Gardner et al.*, 1995]. The data exhibit a pattern which is repeated twice. Two cycles can be defined, starting by very large eruptions (Yn and Wn) and characterized by monotonous changes toward more primitive magma compositions and by temperature increases (from 770°C to 910°C between the Yn and Bi eruptions, and from 850°C to 920°C between the Wn and May 1980 eruptions). Each cycle begins with a large and extremely rapid pressure drop, followed by smaller eruptions associated with weak pressure changes. The two cycles are separated by a rather long lull in explosive activity ($\sim$1000 years) between the Bi and Wn events, during which time the volcano issued lava flows and domes. This transitional phase is characterized by a large pressure increase. At Mount St. Helens, therefore, the consistent pattern seems to be that pressure decreases rapidly whereas phases of pressure increase take much longer. This provides an important clue. A convincing interpretation for Mount St. Helens should account for the systematics in the data, including the existence of two cycles as well as the relationship between pressure and compositional (and hence temperature) changes.

[45] We briefly review problems with a number of possible explanations. Magma withdrawal may affect a small fraction of the reservoir and hence different eruptions may be fed from different levels in a stratified reservoir. However, the samples analyzed by *Gardner et al.* [1995] have homogeneous matrix glass and phenocryst assemblages, save for one particular event, implying that the eruptions tapped a homogeneous magma body. The general trend of chemical and petrological variations, such that the more evolved the magma, the larger the pressure, is the opposite of what is expected of a stably stratified magma chamber. In such a chamber, density must increase with depth, and hence more evolved magmas would be located at the top [*Hildreth*, 1981; *Blake and Ivey*, 1986]. In another class of models, pressure changes are due to variations of reservoir depth [*Gardner et al.*, 1995]. A first problem is that it is very difficult to account for the ascent of large amounts of magma in the short times which separate the Yn-Ye and Wn-We eruptions (Figure 1) [*Miller and Paterson*, 1999; *Petford et al.*, 2000]. In one end-member model, each eruption is fed by its own independent reservoir. Within this framework, the data imply that, in one cycle, successive magma batches get

emplaced at increasingly shallower levels. There is no obvious explanation for the fact that more primitive magmas are able to rise to shallower levels than their evolved counterparts which are less dense. In the other end-member model, a single magma batch moves vertically, feeding eruptions along the way. Replenishment by more primitive magma is required, and the gradual shift toward less evolved compositions implies that the input of primitive magma increases through a cycle. How this is achieved is not specified. None of these models can account for the existence of a second cycle beginning at large depth.

[46] We now evaluate how our model fits the Mount St. Helens observations. As shown by Figures 14a and 14b, the reservoir behavior depends on the values of R_c and H_c. The rather small erupted volumes at Mount St. Helens suggest a reservoir of limited extent. Seismological constraints indicate that this reservoir is probably deeper than 6 km. The present-day edifice has a radius of about 5 km, which puts the reservoir in the zone of compression, such that the critical magmatic overpressure increases with edifice size. Indeed, this is consistent with stratocone growth, as this implies preferential failure of reservoir walls at the axis. As discussed above, we restrict ourselves to a qualitative discussion, postponing a fuller investigation until a range of reservoir shapes has been studied. This is also warranted by the rather large errors in pressure estimates. One can make a good case for Mount St. Helens solely on the basis of the systematics in the observations.

[47] According to our framework, the threshold overpressure for eruption increases as the edifice grows and, conversely, decreases if the edifice gets destroyed (Figure 1). One may note as a starting point that this implies that a pressure increase takes much longer than a pressure decrease, as observed. From the Bi to the Wn eruptions, pressure increased by about 100 MPa in about 1000 years (Figure 1). This period saw voluminous flows and domes which buried older deposits, and the modern edifice was built during that time [*Mullineaux and Crandell*, 1981; *Hopson and Melson*, 1990]. Our model predicts that this should lead to a pressure increase, which is exactly what happened (Figure 1).

[48] The model can also be tested in reverse with destructive events which led to significant reductions of edifice size. A landslide decapitated Mount St. Helens at the end of the Pine Creek period [*Hausback and Swanson*, 1990], after the Pu eruption (Figure 1). The next recorded eruption (Bi) is indeed associated with a smaller pressure. The Wn eruption was very voluminous and was associated with exceptionally large lithic fragments [*Carey et al.*, 1995]. It resulted in partial edifice destruction, as witnessed by the large carter (>500 m deep) which formed at that time [*Hopson and Melson*, 1990]. This led to a significant reduction of edifice load which should have led to a pressure decrease in the reservoir. This is exactly what is observed.

[49] Last, we address the relationship between composition and pressure. In our framework, the reservoir remains at a fixed depth and its temperature varies because of cooling against country rock and because of heating due to replenishment with more primitive and hence hotter magma. An increasing temperature indicates that the effects of replenishment dominate. A phase of falling temperature following an increase can only be accounted for by a drop in replenishment rate. At Mount St. Helens, the significant temperature drop between the Bi and Wn eruptions (from 913°C to 850°C [*Gardner et al.*, 1995]) occurs as pressure increases. This is consistent with a simple hydraulic model for magma flow between a source at pressure P_s and the reservoir at pressure P_r. For a conduit of radius a and distance H between source and reservoir, the flux of magma is equal to

$$Q_{in} = \frac{\pi a^4}{8\mu} \frac{(P_s - P_r) - \rho_m g H}{H}, \tag{18}$$

This shows that an increase of reservoir pressure acts to reduce the flux of magma into the reservoir, and hence to enhance cooling. This accounts for the change toward more evolved magma compositions which took place between the Bi and Wn eruptions. Conversely, a sequence of falling pressures implies an increase of replenishment rate, and hence accounts for the shift toward more primitive compositions in a cycle.

[50] With our model, eruptions with the smallest edifice load are associated with the smallest values of reservoir overpressure. Thus the pressures recorded by their eruptive products are closest to the local pressure in country rock surrounding the reservoir. At Mount St. Helens, the smallest pressure value of 1.6 kbar [*Gardner et al.*, 1995] corresponds to a depth of 6–7 km using the density model of *Williams et al.* [1987]. This is very close to the reservoir depth determined by seismicity studies [*Moran*, 1994].

5. Conclusion

[51] A 1000 m high volcanic edifice exerts a load of about 30 MPa on Earth's surface and induces stresses in the upper crust which are comparable to magmatic overpressures in volcanic reservoirs. If the reservoir is not too deep, this generates stresses on the reservoir walls which may be larger than the surface load itself. There are two important consequences for eruption characteristics. One is that the reservoir walls fail preferentially beneath the top of the edifice, at the top of the reservoir, implying eruptions through a central vent system. The second consequence is to change the magnitude of magmatic overpressure required for reservoir wall fracture. For small reservoirs, this critical overpressure is larger than in the absence of an edifice and increases with edifice size. Conversely, edifice destruction through landslides or explosions, implies a reduction of the critical overpressure. This effect is enhanced for stratovolcanoes with respect to shield volcanoes with gentle slopes. The amplitude of such pressure variations are comparable to, and may even be greater than, tectonic stress levels and may be large enough to be recorded by phenocryst assemblages in crystallizing magma.

Appendix A: Elastic Model

[52] For plane strain, the relationship between stress and strain is

$$\sigma_{xx} = -\left[\lambda\left(e_{xx} + e_{yy}\right) + 2\mu e_{xx}\right], \tag{A1}$$

$$\sigma_{yy} = -\left[\lambda\left(e_{xx} + e_{yy}\right) + 2\mu e_{yy}\right], \tag{A2}$$

$$\sigma_{xy} = -\mu e_{xy}. \tag{A3}$$

such that a tensional stress is negative. Stresses and displacements are calculated from the stress function χ defined by

$$\sigma_{xx} = \frac{\partial^2 \chi}{\partial y^2}, \tag{A4}$$

$$\sigma_{xy} = -\frac{\partial^2 \chi}{\partial y \partial x}, \tag{A5}$$

$$\sigma_{yy} = \frac{\partial^2 \chi}{\partial x^2}. \tag{A6}$$

This function satisfies the biharmonic equation.

[53] Following *Jeffery* [1920], we solve the elastic problem in bipolar coordinates (α, β), so that the free surface and the cavity wall correspond to two surfaces α = const. This system of curvilinear coordinates is defined by the conjugate functions:

$$\alpha + i\beta = \ln\frac{x + i(z + a)}{x + i(z - a)}, \tag{A7}$$

with x, z stand for the Cartesian coordinates, a is the real positive length $\frac{1}{2}O_1O_2$ and i the imaginary number. This system of coordinates is shown in Figure A1 and is such that $\alpha = 0$ for the free surface and $\alpha = \alpha_1$ at the cavity wall. α_1 is defined by

$$\cosh(\alpha_1) = \frac{1}{a_c}. \tag{A8}$$

Coordinates α and β may be calculated using two particular points O_1 and O_2 of Cartesian coordinates (0, a) and (0, -a), respectively (Figure A1),

$$\alpha = \ln\frac{PO_2}{PO_1}, \tag{A9}$$

$$\beta = O_1\widehat{P}O_2. \tag{A10}$$

[54] We first describe the solution obtained by Jeffery for a uniform pressure inside the chamber and zero stress at the free surface and then present the calculation for a uniform load over a disk of radius R_e at the surface.

A.1. An Overpressured Reservoir Beneath a Free Surface

[55] In the bipolar coordinates (α, β), the boundary conditions are

$$\sigma_{\alpha\alpha}(\alpha_1, \beta) = 1, \tag{A11}$$

$$\sigma_{\alpha\beta}(\alpha_1, \beta) = 0, \tag{A12}$$

$$\sigma_{\alpha\alpha}(0, \beta) = 0, \tag{A13}$$

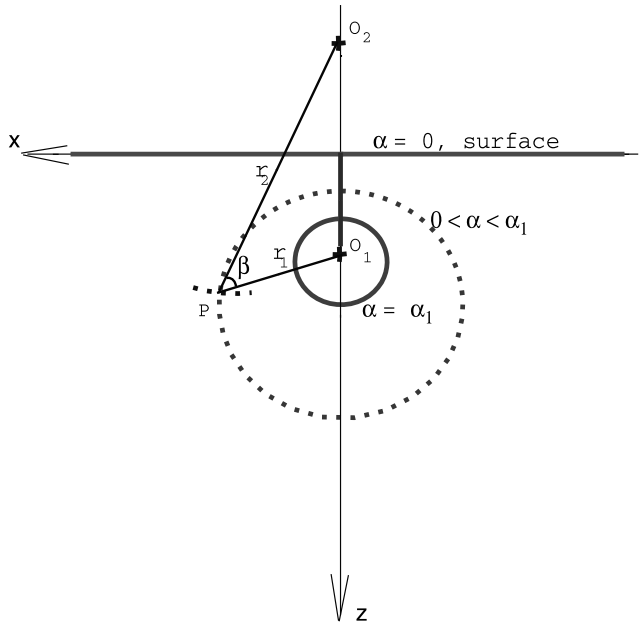

Figure A1. Bipolar coordinates for a half-space with a cylindrical cavity.

$$\sigma_{\alpha\beta}(0, \beta) = 0. \tag{A14}$$

[56] Pressure is normalized by the reservoir overpressure ΔP. In this case, χ is given by

$$\chi = B_0\alpha\sqrt{1 - a_c^2} + \frac{\sqrt{1 - a_c^2}}{\cosh\alpha - \cos\beta}\phi_1(\alpha)\cos(\beta), \tag{A15}$$

where

$$\phi_1(\alpha) = A_1\cosh(2\alpha) + B_1 + C_1\sinh(2\alpha) \tag{A16}$$

[57] Constants B_0, A_1, B_1 and C_1 are set by the boundary conditions

$$B_0 = -\frac{a_c^2}{1 - a_c^2}, \tag{A17}$$

$$A_1 = \frac{a_c^2}{2\sqrt{1 - a_c^2}}, \tag{A18}$$

$$B_1 = -\frac{1}{2}\frac{a_c^2}{\sqrt{1 - a_c^2}}, \tag{A19}$$

$$C_1 = -\frac{a_c^2}{2(1 - a_c^2)} \tag{A20}$$

Stresses are given by

$$\sqrt{1 - a_c^2}\,\sigma_{\alpha\alpha} = B_0\sinh(\alpha)[\cos(\beta) - \cosh(\alpha)] + \phi_1(\alpha) - \cos(\beta)\sinh(\alpha)\dot{\phi}_1(\alpha), \tag{A21}$$

$$\sqrt{1-a_c^2}\,\sigma_{\alpha\beta} = \sin(\beta)\big(B_0 - \dot{\phi}_1(\alpha)\big)[\cos(\beta) - \cosh(\alpha)], \quad \text{(A22)}$$

$$\begin{aligned} 2\sqrt{1-a_c^2}\,\sigma_{\beta\beta} = {} & B_0 \sinh(2\alpha) - \ddot{\phi}_1(\alpha) + 2\phi_1(\alpha) \\ & + 2\cos(\beta)[\cosh(\alpha)\ddot{\phi}_1(\alpha) - B_0 \sinh(\alpha) \\ & - \sinh(\alpha)\dot{\phi}_1(\alpha)] - \cos(2\beta)\ddot{\phi}_1(\alpha). \end{aligned} \quad \text{(A23)}$$

We are particularly interested in the chamber walls, where the hoop stress is

$$\sigma_{\beta\beta}(\alpha_1, \beta) = \frac{1 - a_c^2\cos(2\beta)}{a_c^2 - 1}, \quad \text{(A24)}$$

where

$$\cos\beta = \frac{a_c - \cos\theta}{1 - a_c\cos\theta}. \quad \text{(A25)}$$

[58] The radial displacement is taken to be positive when it is directed toward increasing values of α, i.e., from the exterior to the center of the cavity. This is the opposite of what occurs in the cylindrical coordinate system attached to the cavity center. The radial displacement is given by

$$\begin{aligned} \frac{2G}{a_c}u(\alpha_1, \beta) = {} & -\frac{1}{\big(1-a_c^2\big)} + (3-4\nu)\frac{a_c}{\big(1-a_c^2\big)}\cos\beta \\ & - \frac{a_c(1-2\nu)}{1 - a_c\cos\beta}\left[\frac{a_c}{\big(1-a_c^2\big)}(\sin\beta)^2 + \cos\beta\right]. \end{aligned} \quad \text{(A26)}$$

The tangential deplacement is taken positive when it is along decreasing values of θ:

$$G\frac{\sqrt{1-a_c^2}}{a_c^2}v(\alpha_1, \beta) = (1-\nu)\sin\beta. \quad \text{(A27)}$$

A.2. Load at the Free Surface and Zero Pressure Inside the Reservoir

[59] At Earth's surface, the new boundary condition is

$$\sigma_{zz} = \rho_m g H_e \text{ for } 0 \le r \le R_e. \quad \text{(A28)}$$

The boundary conditions for this problem are

$$\sigma_{\alpha\alpha}(\alpha_1, \beta) = 0, \quad \text{(A29)}$$

$$\sigma_{\alpha\beta}(\alpha_1, \beta) = 0, \quad \text{(A30)}$$

$$\sigma_{\alpha\alpha}(0, \beta) = \frac{\pi - \beta_c}{\pi} - \sum_{n=1}^{\infty}\frac{2}{n\pi}\sin(n\beta_c)\cos(n\beta), \quad \text{(A31)}$$

$$\sigma_{\alpha\beta}(0, \beta) = 0, \quad \text{(A32)}$$

where $\beta_c \in [0;\pi]$ and is given by

$$\cos\beta_c = \frac{a_e^2 - 1 + a_c^2}{a_e^2 + 1 - a_c^2}. \quad \text{(A33)}$$

Here, pressure is normalized by the load of the edifice, $\rho_m g H_e$. The stress function χ may now be written as

$$\chi = B_0\alpha\sqrt{1-a_c^2} + \frac{\sqrt{1-a_c^2}}{\cosh\alpha - \cos\beta}\sum_{n=1}^{\infty}\phi_n(\alpha)\cos(n\beta), \quad \text{(A34)}$$

where

$$\phi_1(\alpha) = A_1\cosh(2\alpha) + B_1 + C_1\sinh(2\alpha), \quad \text{(A35)}$$

and, for $n \ge 2$,

$$\begin{aligned} \phi_n(\alpha) = {} & A_N\cosh((n+1)\alpha) + B_N\cosh((n-1)\alpha) \\ & + C_N\sinh((n+1)\alpha) + D_N\sinh((n-1)\alpha). \end{aligned} \quad \text{(A36)}$$

[60] The integration constants are

$$B_0 = \frac{\pi - \beta_c}{\pi}\frac{a_c^2}{1-a_c^2}, \quad \text{(A37)}$$

$$A_1 = -\frac{\pi - \beta_c}{2\pi}\frac{a_c^2}{\sqrt{1-a_c^2}}, \quad \text{(A38)}$$

$$B_1 = \frac{\pi - \beta_c}{2\pi}\frac{2-a_c^2}{\sqrt{1-a_c^2}}, \quad \text{(A39)}$$

$$C_1 = \frac{\pi - \beta_c}{\pi}\frac{a_c^2}{2\big(1-a_c^2\big)} \quad \text{(A40)}$$

$$\text{for } n \ge 2, A_N = f_n\frac{(n+1) - \cosh(2n\alpha_1) - n\cosh(2\alpha_1)}{2\big[(n+1) + \frac{1}{n-1}\cosh\big(2n\alpha_1\big) - \frac{n^2}{n-1}\cosh(2\alpha_1)\big]}, \quad \text{(A41)}$$

$$B_N = f_n\frac{(n+1) + \frac{n+1}{n-1}\cosh(2n\alpha_1) - \frac{n(n+1)}{n-1}\cosh(2\alpha_1)}{2\big[(n+1) + \frac{1}{n-1}\cosh(2n\alpha_1) - \frac{n^2}{n-1}\cosh(2\alpha_1)\big]}, \quad \text{(A42)}$$

$$C_N = f_n\frac{\sinh(2n\alpha_1) + n\sinh(2\alpha_1)}{2\big[(n+1) + \frac{1}{n-1}\cosh(2n\alpha_1) - \frac{n^2}{n-1}\cosh(2\alpha_1)\big]}, \quad \text{(A43)}$$

$$D_N = f_n\frac{-\frac{n+1}{n-1}\sinh(2n\alpha_1) - \frac{n(n+1)}{n-1}\sinh(2\alpha_1)}{2\big[(n+1) + \frac{1}{n-1}\cosh(2n\alpha_1) - \frac{n^2}{n-1}\cosh(2\alpha_1)\big]} \quad \text{(A44)}$$

f_n are given by

$$f_1 = \sqrt{1-a_c^2}\,\frac{\pi - \beta_c}{\pi}, \quad \text{(A45)}$$

$$f_2 = -\frac{2}{3\pi}\sqrt{1-a_c^2}\sin(\beta_c), \quad \text{(A46)}$$

$$f_3 = -\frac{1}{3\pi}\sqrt{1-a_c^2}\left(\sin(\beta_c) + \frac{1}{2}\sin(2\beta_c)\right), \quad \text{(A47)}$$

$$f_{n+1} = \frac{-\frac{4}{n\pi}\sqrt{1-a_c^2}\sin(n\beta_c) + 2(n-1)(n+1)f_n - (n-2)(n-1)f_{n-1}}{(n+1)(n+2)} \quad \text{(A48)}$$

for $n \geq 3$. Stresses are given by

$$2\sqrt{1-a_c^2}\,\sigma_{\alpha\alpha} = -2B_0\sinh(\alpha)\cosh(\alpha) + 2\phi_1(\alpha) + 2B_0\sinh(\alpha)\cos\beta + \sum_{n=1}^{\infty}\cos(n\beta)\begin{cases}(n+1)(n+2)\phi_{n+1}(\alpha) - 2\cosh(\alpha)(n^2-1)\phi_n(\alpha)\\ +(n-1)(n-2)\phi_{n-1}(\alpha) - 2\sinh(\alpha)\dot{\phi}_n(\alpha)\end{cases} \quad \text{(A49)}$$

$$u_{(\alpha_1,\beta)} = \frac{1}{G}\begin{cases}\dfrac{(\pi-\beta_c)a_c}{2\pi(1-a_c^2)} & \\ -\dfrac{(\pi-\beta_c)a_c^2}{2\pi(1-a_c^2)} & (3-4\nu)\cos\beta \\ +\dfrac{(\pi-\beta_c)a_c^2}{2\pi(1-a_c^2)} & (1-2\nu) \\ -\dfrac{\pi-\beta_c}{2\pi} & (2\nu-1) \\ +2K & (1-\nu) \\ -2(1-\nu) & \sum_{n=2}^{\infty}\dfrac{Q_n}{n(n-1)(n+1)}\end{cases}$$

$$2\sqrt{1-a_c^2}\,\sigma_{\alpha\beta} = -2B_0\cosh(\alpha)\sin(\beta) + B_0\sin(2\beta) - \sum_{n=1}^{\infty}\sin(n\beta)\left[(n+1)\dot{\phi}_{n+1}(\alpha) - 2n\cosh(\alpha)\dot{\phi}_n(\alpha) + (n-1)\dot{\phi}_{n-1}(\alpha)\right] \quad \text{(A50)}$$

$$v_{(\alpha_1,\beta)} = \frac{1}{G}\begin{cases}\dfrac{\pi-\beta_c}{\pi\sqrt{1-a_c^2}} & \left(\dfrac{1-2\nu}{2} - (1-\nu)a_c^2\right)\sin\beta \\ -\dfrac{\pi-\beta_c}{\pi\sqrt{1-a_c^2}} & \dfrac{3-4\nu}{2}\,\dfrac{a_c^2\sin\beta}{1-a_c\cos\beta} \\ +\dfrac{\pi-\beta_c}{\pi\sqrt{1-a_c^2}} & \dfrac{1-2\nu}{4}\,\dfrac{a_c\sin(2\beta)}{1-a_c\cos\beta} \\ +2K\sqrt{1-a_c^2} & (1-\nu)\,\dfrac{\sin\beta}{1-a_c\cos\beta} \\ -2(1-\nu) & \sum_{n=2}^{\infty}\dfrac{Q_n}{n(n+1)}\left[\dfrac{(n+1)}{(n-1)}\sinh((n+1)\alpha_1) - \sinh((n-1)\alpha_1)\right] * \dfrac{\sqrt{1-a_c^2}}{1-a_c\cos\beta} * \sin(n\beta) \\ -2(1-\nu) & \sum_{n=2}^{\infty}\dfrac{Q_n}{n}\sin(n\beta)[\cosh((n+1)\alpha_1) - \cosh((n-1)\alpha_1)]\end{cases} \quad \text{(A56)}$$

$$2\sqrt{1-a_c^2}\,\sigma_{\beta\beta} = B_0\sinh(2\alpha) - \ddot{\phi}_1(\alpha) + 2\phi_1(\alpha) + \cos(\beta)\begin{cases}2\cosh(\alpha)\ddot{\phi}_1(\alpha) - 2B_0\sinh(\alpha) - \ddot{\phi}_2(\alpha)\\ -2\sinh(\alpha)\dot{\phi}_1(\alpha) + 3\phi_2(\alpha).\end{cases} + \sum_{n=2}^{\infty}\cos(n\beta)\begin{cases}2\cosh(\alpha)\ddot{\phi}_n(\alpha) - \ddot{\phi}_{n+1}(\alpha) - \ddot{\phi}_{n-1}(\alpha)\\ -2\dot{\phi}_n(\alpha)\sinh(\alpha)\\ -(n-2)\phi_{n-1}(\alpha) + (n+2)\phi_{n+1}(\alpha).\end{cases} \quad \text{(A51)}$$

[61] The hoop stress at the wall is given by

$$\sigma_{\beta\beta}(\alpha_1,\beta) = \frac{\pi-\beta_c}{\pi}\frac{2-a_c^2}{1-a_c^2} + 4\cos\beta\frac{a_c a_e}{\pi(a_e^2-a_c^2+1)\sqrt{1-a_c^2}} + \frac{4}{a_c^2}\sum_{n=2}^{\infty}\cos(n\beta)\begin{cases}\sinh(n\alpha_1)(2Q_n - Q_{n+1} - Q_{n-1})\\ +\sqrt{1-a_c^2}\cosh(n\alpha_1)(-Q_{n+1} + Q_{n-1}).\end{cases} \quad \text{(A52)}$$

with

$$Q_1 = 2\frac{\pi-\beta_c}{8\pi}\frac{a_c^4}{(1-a_c^2)^{3/2}}$$

$$Q_{n>1} = \frac{n(n+1)f_n}{2\left[(n+1) + \frac{1}{n-1}\cosh(2n\alpha_1) - \frac{n^2}{n-1}\cosh(2\alpha_1)\right]} \quad \text{(A53)}$$

Using the same sign conventions as before, the radial and tangential displacements of the wall are equal to

$$\begin{matrix}\dfrac{a_c(\sin\beta)^2}{1-a_c\cos\beta} \\ \dfrac{\cos\beta}{1-a_c\cos\beta} \\ \dfrac{\cos\beta - a_c}{1-a_c\cos\beta}\end{matrix} \quad \begin{matrix}\\ \\ \\ [(n+1)\sinh((n+1)\alpha_1) - (n-1)\sinh((n-1)\alpha_1)] \\ * \left[n\cos(n\beta) - \dfrac{a_c\sin(n\beta)\sin\beta}{1-a_c\cos\beta}\right]\end{matrix} \quad \text{(A54)}$$

where K is given by

$$K = \sum_{n=2}^{\infty}\frac{Q_n}{(n-1)(n+1)}[\sinh(2n\alpha_1) + n\sinh(2\alpha_1)] \quad \text{(A55)}$$

Appendix B: A Magma-Filled Vertical Crack

[62] In order of characterize the effect of the shape of the reservoir, we consider the example of a vertical crack filled with magma. A crack of length $2z_o$ is initially opened by an overpressure ΔP_i and is then subjected to stresses due to an edifice. The z axis is oriented positively upward and centered at the middle of the crack. The crack width w may be obtained by [see, e.g., *Lister and Kerr*, 1991]

$$\frac{dw}{dz} = \frac{1}{m\pi}\int_{-z_o}^{z_o} p(\sigma)\left(\frac{z_o^2-\sigma^2}{z_o^2-z^2}\right)^{1/2}\frac{d\sigma}{\sigma-z} + \frac{k_2}{(z_o^2-z^2)^{1/2}}, \quad \text{(B1)}$$

where $m = G/(1-\nu)$ and p is the "elastic" pressure (i.e., the difference between the internal magma pressure and the external normal stress). Constant k_2 is determined by

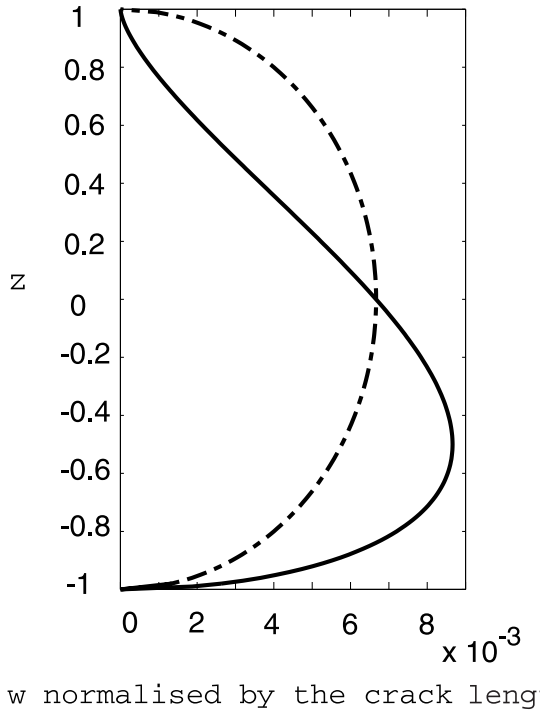

Figure B1. Width for a crack with two distributions of internal overpressure. The dashed line corresponds to a uniform pressure ΔP_i. The plain curve is for a external stress field which depends linearly on depth, which is an approximate representation of the stress field due to an edifice at Earth's surface. The total volume of magma is kept constant in these two calculations in order to illustrate how the load of an edifice acts to deform this particular type of reservoir.

the condition that the crack is closed at its upper end (i.e., $w(z_o) = 0$).

[63] In the initial state, the elastic overpressure $p(\sigma)$ is uniform and equal to some value ΔP_i. Integrating equation (B1), we obtain

$$w(z) = \frac{\Delta P_i}{m}\left(z_o^2 - z^2\right)^{1/2} \tag{B2}$$

[64] We now consider that a volcanic edifice has grown at Earth's surface above the same magma-filled crack. For an incompressible magma, the volume contained within the crack must remain constant. For the sake of simplicity, we approximate the stress distribution due to the edifice in the vicinity of the crack by a linear function, which is valid only if the crack is close enough to the surface. The external stress change due the edifice is thus imposed to be

$$\Delta P_e = \langle \Delta P \rangle + \eta z \tag{B3}$$

where $\eta > 0$ is positive. The elastic overpressure is thus

$$p(\sigma) = \Delta P_f - \langle \Delta P \rangle - \eta\sigma \tag{B4}$$

where ΔP_f is the new overpressure inside the crack, which must be solved for. If the crack is open everywhere, $w(z)$ is now given by

$$w(z) = \frac{\left(z_o^2 - z^2\right)^{1/2}}{2m}\left[2\left(\Delta P_f - \langle \Delta P \rangle\right) - \eta z\right]. \tag{B5}$$

The constraint that the volume of magma inside the crack is conserved implies that

$$\Delta P_f = \Delta P_i + \langle \Delta P \rangle. \tag{B6}$$

This shows that the magma pressure within the crack has been increased by an amount equal to the average value of the normal stress due to the edifice over the length of the crack.

[65] The above calculation is only correct if the crack remains open everywhere, i.e., if $w(z) > 0$ for $|z| < z_o$. This gives a condition relating the crack length, ΔP_i and η,

$$z_o < \frac{2\Delta P_i}{\eta}. \tag{B7}$$

Figure B1 shows the crack width w for the maximum value of z_o. For larger values of z_o, the crack closes at its upper boundary due to the edifice load.

[66] **Acknowledgments.** This study was supported by a grant from INSU/CNRS ("programme PNRN"). The manuscript benefited greatly from the constructive and critical comments of Marcus Bursik, Peter Cervelli, James Gardner, and Olivier Roche.

References

Bacon, C. R., Implications of silicic vent patterns for the presence of large crustal magma chambers, *J. Geophys. Res.*, *90*, 11,243–11,252, 1985.

Barker, S. E., and S. D. Malone, Magmatic system geometry at Mount St. Helens modeled from the stress field associated with posteruptive earthquakes, *J. Geophys. Res.*, *96*, 11,883–11,894, 1991.

Beaumont, C., Foreland basins, *Geophys. J. R. Astron. Soc.*, *65*, 291–329, 1981.

Blake, S., and G. N. Ivey, Density and viscosity gradients in zoned magma chambers, and their influence on withdrawal dynamics, *J. Volcanol. Geotherm. Res.*, *30*, 201–230, 1986.

Blundy, J., and K. Cashman, Ascent-driven crystallisation of dacite magmas at Mount St. Helens, 1980–1986, *Contrib. Mineral. Petrol.*, *140*, 631–650, 2001.

Carey, S., J. Gardner, and H. Sigurdsson, The intensity and magnitude of Holocene Plinian eruptions from Mount St. Helens volcano, *J. Volcanol. Geotherm. Res.*, *66*, 185–202, 1995.

Dahm, T., Numerical simulations of the propagation path and the arrest of fluid-filled fractures in the Earth, *Geophys. J. Int.*, *141*, 623–638, 2000.

Davis, P. M., Surface deformation due to inflation of an arbitrarily oriented triaxial ellipsoidal cavity in an elastic half-space, with reference to Kilauea Volcano, Hawaii, *J. Geophys. Res.*, *91*, 7429–7438, 1986.

Gardner, J. E., M. Rutherford, S. Carey, and H. Sigurdsson, Experimental constraints on pre-eruptive water contents and changing magma storage prior to explosive eruptions of Mount St. Helens volcano, *Bull. Volcanol.*, *57*, 1–17, 1995.

Hausback, B. P., and D. A. Swanson, Record of prehistoric debris avalanches on the north flank of Mount St. Helens volcano, Washington, *Geosci. Can.*, *17*, 142–145, 1990.

Hildreth, W., Gradients in silicic magma chambers: Implications for lithospheric magmatism, *J. Geophys. Res.*, *86*, 10,153–10,192, 1981.

Hildreth, W., and M. A. Lanphere, Potassium-argon geochronology of a basalt-andesite-dacite arc system: The Mount Adams volcanic field, Cascade Range of southern Washington, *Geol. Soc. Am. Bull.*, *106*, 1413–1429, 1994.

Hopson, C. A., and W. G. Melson, Compositional trends and eruptive cycles at Mount St. Helens, *Geosci. Can.*, *17*, 131–141, 1990.

Jeffery, G. B., Plane stress and strain in bipolar co-ordinates, *Trans. R. Soc. London, Ser. A*, *221*, 265–293, 1920.

Lees, J. M., The magma system of Mount St. Helens: Non-linear high resolution P-wave tomography, *J. Volcanol. Geotherm. Res.*, *53*, 103–116, 1992.

Lister, J. R., and R. C. Kerr, Fluid-mechanical models of crack propagation and their application to magma transport in dikes, *J. Geophys. Res.*, *96*, 10,049–10,077, 1991.

Love, A. E. H., *A Treatise on the Mathematical Theory of Elasticity*, 643 pp., Dovers, Mineola, N. Y., 1944.

McLeod, P., and S. Tait, The growth of dykes from magma chambers, *J. Volcanol. Geotherm. Res.*, *92*, 231–246, 1999.

McTigue, D. F., Elastic stress and deformation near a finite spherical magma body: Resolution of the point source paradox, *J. Geophys. Res.*, *92*, 12,931–12,940, 1987.

Metz, J. M., and G. A. Mahood, Precursors to the Bishop Tuff eruption: Glass Mountain, Long Valley, California, *J. Geophys. Res.*, *90*, 11,121–11,126, 1985.

Metz, J. M., and G. A. Mahood, Development of the Long Valley, California, magma chamber recorded in precaldera rhyolite lavas of Glass Mountain, *Contrib. Mineral. Petrol.*, *106*, 379–397, 1991.

Miller, R. B., and S. R. Paterson, In defense of magmatic diapirs, *J. Struct. Geol.*, *21*, 1161–1173, 1999.

Mogi, K., Relations between the eruptions of various volcanoes and the deformations of the ground surfaces around them, *Bull. Earthquake Res. Inst. Univ Tokyo*, *36*, 99–134, 1958.

Moran, S. C., Seismicity at Mount St. Helens, 1987–1992: Evidence for repressurization of an active magmatic system, *J. Geophys. Res.*, *99*, 4341–4354, 1994.

Muller, J. R., G. Ito, and S. J. Martel, Effects of volcano loading on dike propagation in an elastic half-space, *J. Geophys. Res.*, *106*, 11,101–11,113, 2001.

Mullineaux, D. R., Summary of pre-1980 tephra-fall deposits erupted from Mount St. Helens, Washington State, U.S.A., *Bull. Volcanol.*, *48*, 17–26, 1986.

Mullineaux, D. R., and D. R. Crandell, The eruptive history of Mount St. Helens, in *The 1980 Eruptions of Mount St. Helens, Washington*, edited by P. W. Lipman and D. R. Mullineaux, U.S. Geol. Surv. Prof. Pap., 1250, 3–15, 1981.

Nunn, J. A., and N. H. Sleep, Thermal contraction and flexure of intracratonal basins: A three dimensional study of the Michigan basin, *Geophys. J. R. Astron. Soc.*, *76*, 587–635, 1984.

Okada, Y., Surface deformation due to shear and tensile faults in a half-space, *Bull. Seismol. Soc. Am.*, *75*, 1135–1154, 1985.

Petford, N., A. R. Cruden, K. J. W. McCaffrey, and J.-L. Vigneresse, Granite magma formation, transport and emplacement in the Earth's crust, *Nature*, *408*, 669–673, 2000.

Pinel, V., and C. Jaupart, The effect of edifice load on magma ascent beneath a volcano, *Philos. Trans. R. Soc. London, Ser. A*, *358*, 1515–1532, 2000.

Rutherford, M. J., and J. D. Devine, The may 18, 1980, eruption of Mount St. Helens, 3, Stability and chemistry of amphibole in the magma chamber, *J. Geophys. Res.*, *93*, 11,949–11,959, 1988.

Siebert, L., H. Glicken, and T. Ui, Volcanic hazards from Bezymianny- and Bandai-type eruptions, *Bull. Volcanol.*, *49*, 435–459, 1987.

Tait, S., C. Jaupart, and S. Vergniolle, Pressure, gaz content and eruption periodicity of a shallow, crystallising magma chamber, *Earth Planet. Sci. Lett.*, *92*, 107–123, 1989.

Tsuchida, E., Y. Saito, I. Nakahara, and M. Kodama, Stresses in a semi-infinite elastic body containing a prolate spheroidal cavity subjected to an axisymmetric pressure, *Bull. JSME*, *25*, 891–897, 1982.

Valko, P., and M. J. Economides, *Hydraulic Fracture Mechanics*, 298 pp., John Wiley, New York, 1995.

Van Wyk de Vries, B., and R. Matela, Styles of volcano-induced deformation: Numerical models of substratum flexure, spreading and extrusion, *J. Volcanol. Geotherm. Res.*, *81*, 1–18, 1998.

Williams, D. L., and C. A. Finn, Analysis of gravity data in volcanic terrain and gravity anomalies and subvolcanic intrusions in the Cascade Range, U.S.A., and at other selected volcanoes, in *The Utility of Regional Gravity and Magnetic Anomaly Maps*, edited by W. Hinze, pp. 361–374, Soc. of Explor. Geophys., Tulsa, Okla., 1985.

Williams, D. L., G. Abrams, C. Finn, D. Dzurisin, D. Johnson, and R. Denlinger, Evidence from gravity data for an intrusive complex beneath Mount St. Helens, *J. Geophys. Res.*, *92*, 10,207–10,222, 1987.

C. Jaupart and V. Pinel, Institut de Physique du Globe de Paris, 4 Place Jussieu, 75252 Paris cedex 05, France. (jaupart@ipgp.jussieu.fr; pinel@ipgp.jussieu.fr)